Palaeogeography, Palaeoclimatology, Palaeoecology 331–332 (2012) 75–89

Contents lists available at SciVerse ScienceDirect

Palaeogeography, Palaeoclimatology, Palaeoecology

journal homepage: www.elsevier.com/locate/palaeo

Late Pleistocene history of turbidite sedimentation in a submarine canyon off the northern Great Barrier Reef, Australia

Jody M. Webster [a,b,*], Robin J. Beaman [c], Ángel Puga-Bernabéu [a,d], Deane Ludman [b], Willem Renema [e,f], Raphael A.J. Wust [b], Nicholas P.J. George [b], Paula J. Reimer [e,f], Geraldine E. Jacobsen [g], Patrick Moss [h]

[a] Geocoastal Research Group, School of Geosciences, The University of Sydney, NSW 2006, Australia
[b] School of Earth and Environmental Sciences, James Cook University, Townsville, QLD 4811, Australia
[c] School of Earth and Environmental Sciences, James Cook University, PO Box 6811, Cairns QLD 4870, Australia
[d] Departamento de Estratigrafía y Paleontología, Universidad de Granada, 18002 Granada, Spain
[e] Nederlands Centrum voor Biodiversiteit, Leiden, PO Box 9517 RA, The Netherlands
[f] School of Geography, Archaeology and Palaeoecology (GAP), Queen's University Belfast, Belfast, BT7 1NN, Northern Ireland, UK
[g] Institute for Environmental Research, Australian Nuclear Science and Technology Organisation, Locked Bag 2001, Kirrawee DC, NSW 2232, Australia
[h] School of Geography, Planning & Environmental Management The University of Queensland Brisbane QLD 4072, Australia

ARTICLE INFO

Article history:
Received 19 September 2011
Received in revised form 19 February 2012
Accepted 26 February 2012
Available online 7 March 2012

Keywords:
Great Barrier Reef
Submarine canyons
Turbidites
Sediment transport
Late Pleistocene
Sea level change

ABSTRACT

Cores from slopes east of the Great Barrier Reef (GBR) challenge traditional models for sedimentation on tropical mixed siliciclastic-carbonate margins. However, satisfactory explanations of sediment accumulation on this archetypal margin that include both hemipelagic and turbidite sedimentation remain elusive, as submarine canyons and their role in delivering coarse-grained turbidite deposits, are poorly understood. Towards addressing this problem we investigated the shelf and canyon system bordering the northern Ribbon Reefs and reconstructed the history of turbidite deposition since the Late Pleistocene. High-resolution bathymetric and seismic data show a large paleo-channel system that crosses the shelf before connecting with the canyons via the inter-reef passages between the Ribbon Reefs. High-resolution bathymetry of the canyon axis reveals a complex and active system of channels, sand waves, and local submarine landslides. Multi-proxy examination of three cores from down the axis of the canyon system reveals 18 turbidites and debrites, interlayered with hemipelagic muds, that are derived from a mix of shallow and deep sources. Twenty radiocarbon ages indicate that siliciclastic-dominated and mixed turbidites only occur prior to 31 ka during Marine Isotope Stage (MIS) 3, while carbonate-dominated turbidites are well established by 11 ka in MIS1 until as recently as 1.2 ka. The apparent lack of siliciclastic-dominated turbidites and presence of only a few carbonate-dominated turbidites during the MIS2 lowstand are not consistent with generic models of margin sedimentation but might also reflect a gap in the turbidite record. These data suggest that turbidite sedimentation in the Ribbon Reef canyons, probably reflects the complex relationship between the prolonged period (>25 ka) of MIS3 millennial sea level changes and local factors such as the shelf, inter-reef passage depth, canyon morphology and different sediment sources. On this basis we predict that the spatial and temporal patterns of turbidite sedimentation could vary considerably along the length of the GBR margin.

1. Introduction

Traditionally, sedimentation on continental margins has been interpreted within the framework of idealized siliciclastic or carbonate systems, depending on whether rivers or shallow marine carbonate producers dominate supply (Posamentier and Vail, 1988). For tropical mixed siliciclastic-carbonate systems relatively common in the geologic record (Mount, 1984), the widely accepted paradigm of *reciprocal* sedimentation (Wilson, 1967; Dolan, 1989; Schlager et al., 1994) states that sea level strongly influences shelf, slope and basin sedimentation, with delivery of siliciclastic sediments to the slope and basin being highest during lowstands. In contrast, carbonate sediments dominate during transgressions and highstands as sea level flood the shelf, switching on neritic carbonate production that is exported basinward. However, recent work on the slope and basin of the largest extant tropical mixed siliciclastic-carbonate system – the Great Barrier Reef (GBR) – has challenged this traditional view.

Work on hemipelagic sediment cores from the slope and basin offshore the central and northern GBR, argues for a new model of margin sedimentation (*transgressive shedding*) (e.g. Dunbar and Dickens, 2003; Dunbar et al., 2000). A key finding of this model is that, in

* Corresponding author at: Geocoastal Research Group, School of Geosciences, The University of Sydney, NSW 2006, Australia. Tel.: +61 2 9036 6538; fax: +61 2 9351 0184.
E-mail address: jody.webster@sydney.edu.au (J.M. Webster).

0031-0182/$ – see front matter © 2012 Elsevier B.V. All rights reserved.
doi:10.1016/j.palaeo.2012.02.034

contrast to the widely accepted *reciprocal* model, maximum siliciclastic fluxes to the slope over the last 30 ka occurred during the late transgression ca. 11–7 ka, rather than when sea level was at a lowstand before 18 ka. This pattern appears to be consistent along a large portion of the northeast Australian margin regardless of significant regional climate and physiographic variations. Dunbar and Dickens (2003) offered two general explanations of these observations: (1) that climate change induced highly variable riverine discharge over the past 30 ky with a prominent maximum coincident with late transgression; or (2) the shelf stores large quantities of siliciclastic sediment during lowstand and releases this material to the slope during late transgression. A second key finding, also at odds with the *reciprocal* model, is that accumulation of siliciclastic and carbonate sediments appears to vary coevally (Page et al., 2003; Francis et al., 2007). Bostock et al. (2009) recognized a similar *coeval* (after Francis et al., 2007) pattern of hemipelagic siliciclastic and carbonate sedimentation in cores from the southern GBR, but in this case the maximum flux was recorded earlier in the transgression.

It is important to note that these new models of GBR margin sedimentation pertain specifically to sedimentation away from submarine canyons and turbidites, or lacked the high-resolution bathymetry data needed to constrain it (Bostock et al., 2009). Previous Seabeam multibeam bathymetry and GLORIA sidescan surveys (Hughes-Clarke, 1994) revealed several regions between latitude 14°S and 17°S characterized by well developed submarine canyons and high seafloor backscattering, interpreted as coarse-grained sediment gravity flows (Dunbar et al., 2000). Furthermore, Ocean Drilling Program (ODP) Leg 133 coring confirmed that the delivery of coarse-grained sediments to the slopes and basin is an important component of GBR margin sedimentation. Watts et al. (1993) observed more than 2000 turbidites, debris-flow and slump deposits (herein termed gravity deposits) since the Miocene from Site 823 in the central axis of the Queensland Trough. Detailed sedimentologic investigations of this and other sites (e.g. ODP Site 821 on the upper slope) revealed a mix of abundant quartz and other terrigenous components, bioclastic grains and neritic foraminifers (Montaggioni and Venec-Peyré, 1993) clearly sourced from neritic shelves, and planktonic foraminifers re-worked from the slopes and/or drowned shelves. Watts et al. (1993) considered the influx of quartz and bioclastic sediments in the turbidites to be the best lowstand indictors. However, no one-for-one relationship could be established between sea level fluctuations and the composition of the gravity deposits, in part due to a lack of chronologic control, leaving the authors to argue a complex interplay of tectonic movements, fluctuations of sea level and sedimentologic factors (i.e. slope instability) controlled the nature of these deposits.

While focused on patterns of hemipelagic sedimentation, Dunbar et al. (2000) also discussed the relationship of turbidites in piston cores from the Queensland Trough and sea level change over the last 100 ka (e.g. Fig. 15 in Dunbar et al., 2000). They argued that the turbidite frequency in the Queensland Trough was probably highest during the lowstands, similar to conclusions reached by Watts et al. (1993), and also in an unpublished sedimentologic study (Blakeway, 1991) of canyon cores for the Ribbon Reef region adjacent to the Lark gravity flow (Dunbar et al., 2000). However, these studies lacked the precise chronologic control necessary to accurately constrain the timing of turbidite deposition, and thus firmly establish their relationship to sea level or other factors. Nor at the time of these studies were modern high-resolution multibeam data available for the margin making it difficult to place these cores within an accurate geomorphic context, so crucial for accurately reconstructing gravity deposit processes and sediment pathways.

It is clear that despite significant progress in understanding hemipelagic sedimentation on the GBR margin, our understanding of the processes that control the transport and deposition of coarse-grained siliciclastic and carbonate sediments on this archetypal system, remains elusive. For example, in the context of the highest hemipelagic siliciclastic flux observed during the early transgression, would we also expect to see siliciclastic turbidites dominate at this time? In general terms, the generic or *reciprocal* model would predict that siliciclastic turbidites would dominate during lowstands and carbonates during highstands (Posamentier and Vail, 1988). However, in light of the new observations and models of GBR sedimentation and others further south off Fraser Island (Boyd et al., 2008; Schröder-Adams et al., 2008), significant questions remain about mass wasting processes and how the coarse-grained gravity deposits might (or might not) be superimposed on the temporal patterns of siliciclastic and carbonate hemipelagic sedimentation (Dunbar and Dickens, 2003). We address these questions directly by investigating the history of turbidite sedimentation in a single submarine canyon bordering the northern GBR, adjacent to the Ribbon Reefs (RR).

Based on new radiometric, sedimentologic, geochemical data from cores and newly acquired high-resolution multibeam and seismic data, we: (1) show that the coarse-grained gravity deposits in the canyon are composed of carbonate and siliciclastic sediments and sourced from the shallow shelf and/or re-working of deeper slopes; (2) confirm the canyons have been active since the Late Pleistocene to the late Holocene, and are superimposed on the regional pattern of hemipelagic sedimentation; (3) show that the observed peak into siliciclastic dominated turbidites is co-incident with millennial-scale sea level changes during the end of MIS3 (34–31 ka); and (4) argue that in general the influx of coarse siliciclastic sediment is strongly influenced by prolonged millennial-scale sea level changes and their interactions with local physiography, particularly reef morphology and the depth of the inter-reef passages and shelf.

2. Methods

Bathymetry data for the entire Ribbon Reef region were collected using an EM300 (30 kHz) multibeam echo sounder during the SS07/2007 *RV Southern Surveyor* cruise (Webster et al., 2008). The data were integrated with all available bathymetry data (Beaman, 2010 for methods and data) to produce a comprehensive digital elevation model (DEM) at a resolution of 100 m (Fig. 1). A hydrological drainage analysis using ArcGIS was performed on the DEM assuming an equal distribution of rainfall over the surface in order to highlight the likely paleo-drainage channels crossing the shelf. Seismic reflection data were also acquired from the GBR shelf using a Topas PS18 on the SS09/2008 *RV Southern Surveyor* cruise to map the subsurface characteristics of any surface channels.

Over 40 short piston cores were collected on previous *RV Franklin* cruises (FR5/90 and FR4/92) forming a dense grid over the North Queensland slope and basin (see Fig. 3 in Francis et al., 2007). However, most of the previous work on these cores has focused on areas away from known canyons. We selected three piston cores (PC21, PC20, PC19), from 137 to 190 cm in length, for a more detailed investigation because: (1) previous sedimentologic observations confirmed the presence of prominent sandy turbidite deposits (Blakeway, 1991; Hughes-Clarke, 1994); (2) they form a southeast transect between 1982 and 2200 m water depth down the axis of the largest canyon (Canyon 1, Figs. 1, 3) and are adjacent to well-studied hemipelagic cores (PC22, 23, 27a, PC29; Fig. 2 in Dunbar and Dickens, 2003) in the inter-canyon areas; and (3) with the recent acquisition of the high-resolution multibeam data, these cores can now be placed within an accurate geomorphic context, including likely sediment pathways from the shelf to the basin.

To identify and fully characterize all turbidites and interlayered hemipelagic muds, visual logging, X-radiography, magnetic susceptibility, and color reflectance were undertaken (see Supplementary Table 1 for raw data). This was followed by discrete samples for measurement of sediment texture, carbonate content, and coarse-grained composition analyses at 5–10 cm intervals, and pollen contents at 10–40 cm intervals down core. Grain properties on ~0.25 mg samples were measured

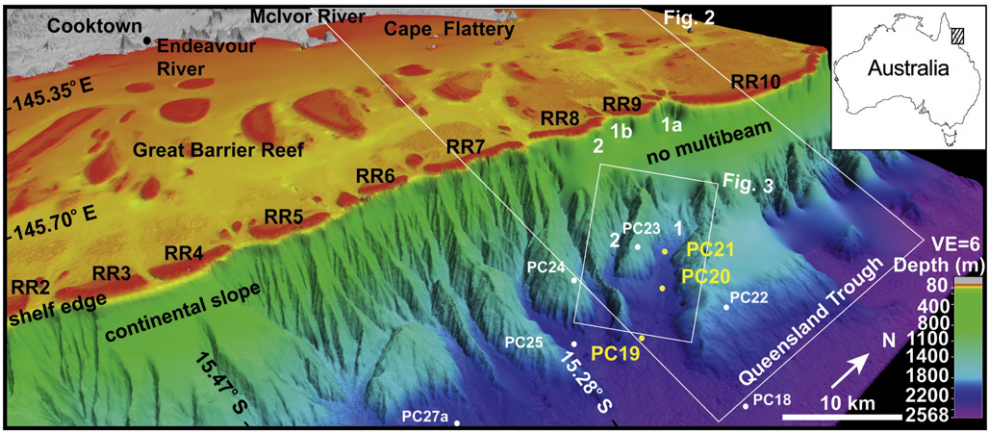

Fig. 1. Composite topographic/bathymetric 100 m grid of the Ribbon Reef (RR) region. The white boxes show close ups of the shelf (Fig. 2), main canyon system (Canyons 1 and 2; Fig. 3) and location of the sediment cores (Fig. 3) that are the focus of this study. VE refers to the vertical exaggeration.

using a Malvern TM Mastersizer-2000 laser particle size analyzer. Textural properties (mean grain size, sorting, skewness and kurtosis) were calculated using standard techniques (Folk and Ward, 1957).

Calcium carbonate content ($CaCO_3$%) was estimated by measuring the total carbon of the samples (0.25–1.3 g) using an Elementar VarioMAX CNS analyzer. This technique does not distinguish between inorganic and organic carbon but takes measurements of 6 representative samples using the traditional Karbonate–Bombe technique that are consistent (within 10%) with CNS-derived $CaCO_3$ measurements. Grain compositions were estimated by point counting >300 grains from >250 μm sieved size fractions within twelve categories (planktonic foraminifera, benthic foraminifera, siliciclastic grains (i.e. quartz, lithic fragments), echinoids, bryozoans, spicules, pteropods, gastropods, bivalves, coralline algae, coral fragments and unidentified

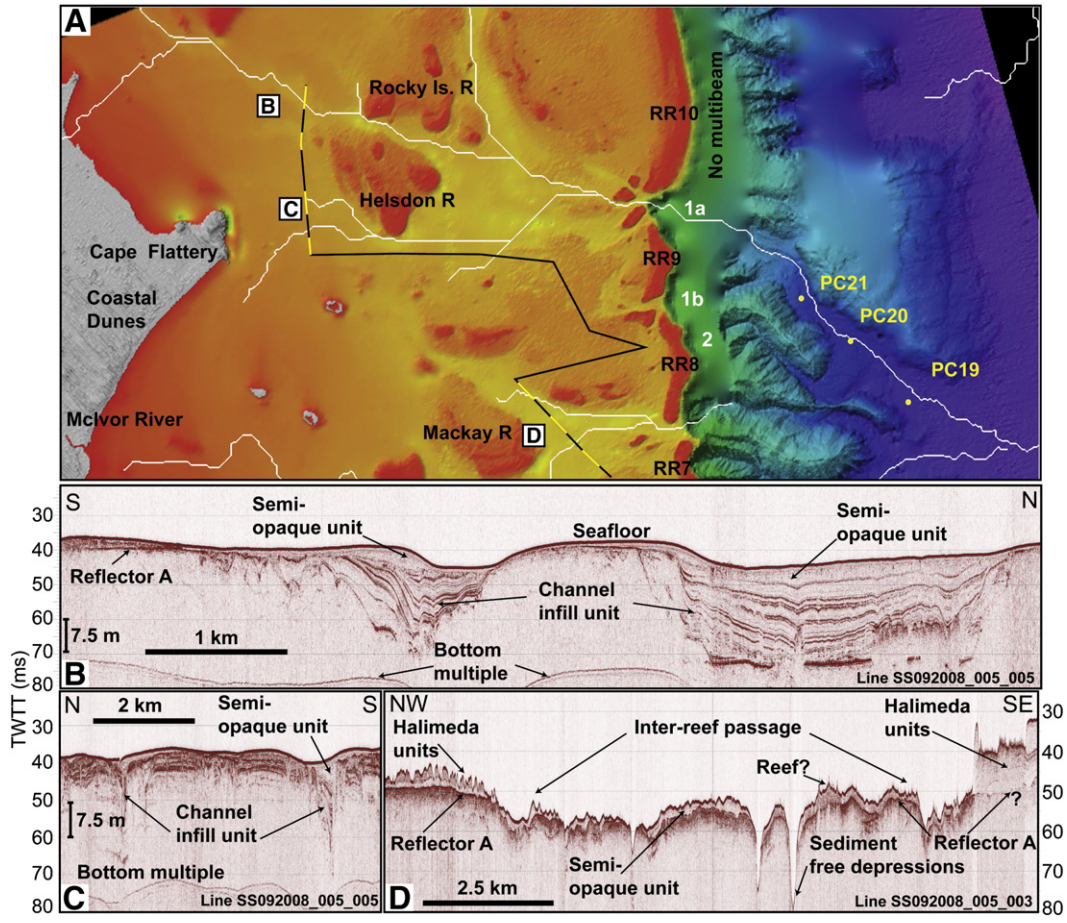

Fig. 2. A: Plan view image of the 100 m bathymetry grid showing the margin east of Cape Flattery. The white lines represent surface drainage pathways across the shelf, through the inter-reef passages (i.e. RR10-RR9) and into the canyons. The black line is a high-resolution Topas PS18 seismic line crossing the shelf, and the yellow/black intervals show the positions of the seismic profiles. B: Seismic line (Line SS092008_005_005) across the shelf showing buried paleochannels beneath two surface channels. C: Further south, the seismic line crosses two smaller surface channels and two buried paleochannels. D: Seismic line (Line SS092008_005_003) crossing the landward side of the inter-reef passage between RR8 and RR7. The inset vertical scale bar was converted to depth by assuming a p-wave velocity of 1500 m s^{-1} (TWTT).

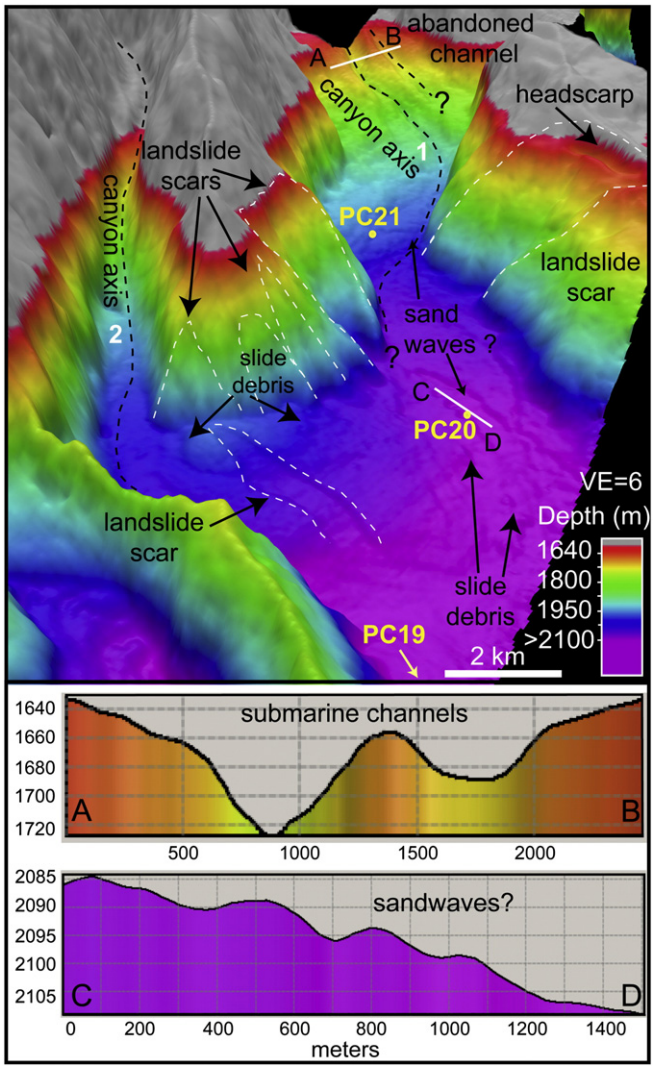

Fig. 3. High-resolution 40 m bathymetry grid of the Ribbon Reef (RR) canyon study area. The view looks up the Canyon 1 and 2 axes towards the RR10-9 inter-reef passage and also shows the core locations. PC21 is located in the proximal reaches of Canyon 1 adjacent to the outer bend of the main channel axis. PC20 is located further down the Canyon 1 axis where the seabed is potentially influenced by sand wave and landslide deposits. PC19 is the most distal core and is potentially influenced by sediments transported down both Canyons 1 and 2.

carbonate fragments). The taxonomic composition of benthic foraminifera was assessed to provide information about their original life habitats.

Magnetic susceptibility was measured using an Azeotech MF CoreScan Magnasat system. Readings were taken at a frequency of 4500 Hz and a gain of 10,000. This instrument has a replication error of 5–10% with results expressed as 10^{-4} SI scale units. Core spectral color was measured every 2.5 mm using a Gretag Macbeth Spectrolino spectrometer, with a ceramic plate (BCA — Gretag Macbeth) as the white standard. The spectral length ranges from 380 to 730 nm with a spectral resolution of 3 nm bandpass filter width which was resampled to 10 nm. The 650 nm (red spectrum) wave length was used here after Rein and Sirocko (2002). X-radiographs were taken using a Phillips Diagnostic imager set at 10 mAs (milliampere second) and 70 kV (kilo volt).

Turbidite chronology comes from 20 ages provided by accelerator mass spectrometry (AMS) radiocarbon analyses of >300 well-preserved, individual mixed layer (<100 m water depth habitat) planktonic foraminfera (*Globigerinoides ruber*, *Globigerinoides trilobus* and *Globigerinoides conglobatus*) sampled mainly from intervals within the hemipelagic muds directly underlying each turbidite deposit (Figs. 5–7). This dating approach (Goldfinger et al., 2007) provides an accurate maximum age of turbidite emplacement without the ambiguity of distinguishing between top of the turbidite (i.e. the "tail") and overlying muds. All radiocarbon ages <48,000 ^{14}C yrs BP were converted to calibrated ages (ka) using CALIB 6.0.1 (Marine09.14C "global" marine calibration dataset described in Reimer et al., 2009) with ages ranges reported with 2σ errors. This calibration takes into account a correction for the average ocean reservoir (R) (400 ^{14}C yrs) as well as a mean local deviation (ΔR) for NE Australia of 12 ± 13 ^{14}C yrs calculated from the Marine Radiocarbon Reservoir Corrections database (Reimer and Reimer, 2010). After first correcting for similar average ocean reservoir (R) (400 yrs) affects, the two ages >48,000 ^{14}C ka were converted to approximate calibrated ages (ka) using CalPal-2007 (Weninger et al., 2007). However, given the very old ages and small sample sizes, these measurements more conservatively represent "background" ages at least older than about 50 ka.

3. Results

3.1. Shelf and canyon morphology

The integrated 100 m DEM shows the relationships between the shelf, Ribbon Reefs, inter-reef passages and the submarine canyon system east of Cape Flattery (Figs. 1, 2). A hydrological analysis of the DEM shows a surface drainage system that can be traced continuously across the inner-shelf around the Rocky Island and Helsdon Reefs, then across the shelf before exiting into the Ribbon Reef canyon system via the inter-reef passage between RR10-9 (Fig. 2A). A similar network of surface drainage channels is also observed on the shelf adjacent to the present McIvor River, before wrapping around the south side of Mackay Reef and then exiting through the inter-reef passage between RR8-7 (Figs. 1, 2A).

The new high-resolution seismic data across the surface drainage pathways confirms the presence of two large buried paleo-channels up to 2.2 km wide and about 20 m deep on the inner-shelf west of Rocky Island Reef (Fig. 2B). Along with two smaller paleo-channels observed west of Helsdon Reef (Fig. 2C), this represents the largest paleo-channel system imaged on the northern GBR shelf. Complex internal reflector geometry (symmetrical and asymmetrical) and characteristics are consistent with other systems in the GBR also interpreted as large buried paleo-rivers formed during lower sea levels (e.g. paleo-Burdekin, Fielding et al., 2003; paleo-Fitzroy, Ryan et al., 2007). However, unlike the paleo-Burdekin and Fitzroy systems, which begin near their modern river mouths, there is no significant modern river near Cape Flattery. Due to a lack of seismic data we are unable to continuously trace the path of the paleo-channels in the subsurface across the outer-shelf and through the inter-reef passage between RR10-9. However, a possible connection is plausible when the surface drainage analysis is considered in the context of a seismic crossing of the outer shelf further south adjacent to the RR8-7 inter-reef passage (Fig. 2D). Here the bathymetry and seismic data show an 8 km wide, complex network of incised channels and depressions between two bathymetric highs characterized by early Holocene (11–10 ka) *Halimeda* deposits growing off a prominent sub-bottom reflector (Marshall and Davies, 1988). This reflector (i.e. "Reflector A") (Orme and Salama, 1988) has been mapped regionally and represents the late Pleistocene erosional unconformity that formed during lower sea levels, and then was subsequently transgressed during the early Holocene (Marshall and Davies, 1988). Within the RR8-7 inter-reef passage, the channels and depressions are generally sediment free or covered by only a thin layer of seismically semi-opaque Holocene sediments, consistent with other inter-reef passages further south (e.g. RR5; Marshall and Davies, 1988) and north (e.g. Cooks Passage) (Orme and Salama, 1988).

The regional morphology of the Ribbon Reef canyon system has been described in detail by Puga-Bernabéu et al. (2011). They recognize

two main types of submarine canyons based on their incision depth: shelf-incised canyons (Type 1) (e.g. 70–100 m, RR5, RR7) and slope-confined canyons (Type 2) (e.g. 450–630 m, RR4-3). According to the degree of connection with the shelf, the shelf-incised canyons either range from reef-blocked to fully shelf-connected (Puga-Bernabéu et al., 2011). In the primary study area (Fig. 1), the inter-reef passages between RR10-9 (50–70 m), and possibly RR9-8 (40–65 m), feed directly into the upper canyon branches 1a and 1b (Fig. 1), potentially sourcing sediments throughout the main Canyon 1 axis. Canyon incision up to the shelf break at 80 m seaward of RR8 and RR9 (i.e. reef-blocked) indicates that sediments could also be derived from the reefs themselves and the narrow shelf edge seaward of these reefs. Therefore any sediments derived directly from RR8 could be sourced via Canyon 2 before merging into the main canyon axis in the distal section of Canyon 1 adjacent to PC19 (Fig. 2A).

Analysis of a smaller canyon area DEM at 40 m resolution (Fig. 3) provides a detailed 3D view of the complex morphology and processes operating within Canyons 1 and 2, as well as the context of the three cores. A submarine channel, 700 m wide and incising up to 70 m below the main canyon floor (Fig. 3, profiles A–B), occurs in the upper canyon. This channel, also observed in the hydrological drainage analysis (Fig. 2A), can be clearly traced 10 km down the canyon, locally forming well-developed thalwegs (Fig. 3). Large bedforms, up to 8 m high and 200–300 m long, are observed in the canyon axis (Fig. 3, profiles C–D). These features are consistent with the sandwaves (sediment waves) described regionally (Puga-Bernabéu et al., 2011) and interpreted as evidence of relatively recent canyon activity (Wynn and Stow, 2002). Evidence for large landslides, up to 2.4 km across, comes from six wedge-shaped scars preserved in the canyon side walls and floor, and also from downslope slide debris (Fig. 3).

3.2. Turbidite stratigraphy, texture and composition

We recognize 18 distinct sandy deposits (labeled T1, T2 etc.) interbedded with hemipelagic mud deposits in the three cores PC21, PC20 and PC19 (Figs. 4–7), similar to earlier descriptions by Blakeway (1991). Based on our re-investigation of these deposits, we provide a summary of their main stratigraphic, textural, compositional and chronologic characteristics below, first the proximal and then distal cores. However, full details (structures, grains size, sorting, skewness, kurtosis, % carbonate, specific grain components) of each of the coarse-grained deposits are also presented in Tables 1 and 2.

The sandy deposits vary considerably from poor- to well-sorted, very fine- to medium-grained sands and local gravels with few examples showing fining-upwards grading (e.g. PC21 T2, PC20 T5; Fig. 6J). Visual logging and X-radiographs confirm that these deposits are mainly characterized by structure-less or "massive" sandy deposits (Cantero et al., 2012) bounded by sharp, erosive bases, and in a few cases parallel- and cross-laminations (e.g. Figs. 5–7; PC20 T2, PC19 T3). With two exceptions (T4 and T3 in PC21) we suggest these deposits most likely reflect turbidite deposition (Shanmugam, 2002). This is also consistent with previous interpretations of these cores (Blakeway, 1991; Hughes-Clarke, 1994), and the terminology used to describe sandy turbidite deposits elsewhere in the region (e.g. Dunbar et al., 2000). Within the Ribbon Reef canyon cores, the number and thickness of the turbidites vary between nine fine- to medium-grained turbidites, and 24 cm thick, in the proximal cores (PC21, 20) while only three thin (>10 cm) laminated fine-grained turbidites in the more distal core PC19 (Table 2).

Sediments on the northeast Australia margin essentially reflect two main sources — terrigenous siliciclastic and biogenic carbonates (Dunbar et al., 2000; Page et al., 2003; Francis et al., 2007). Based on

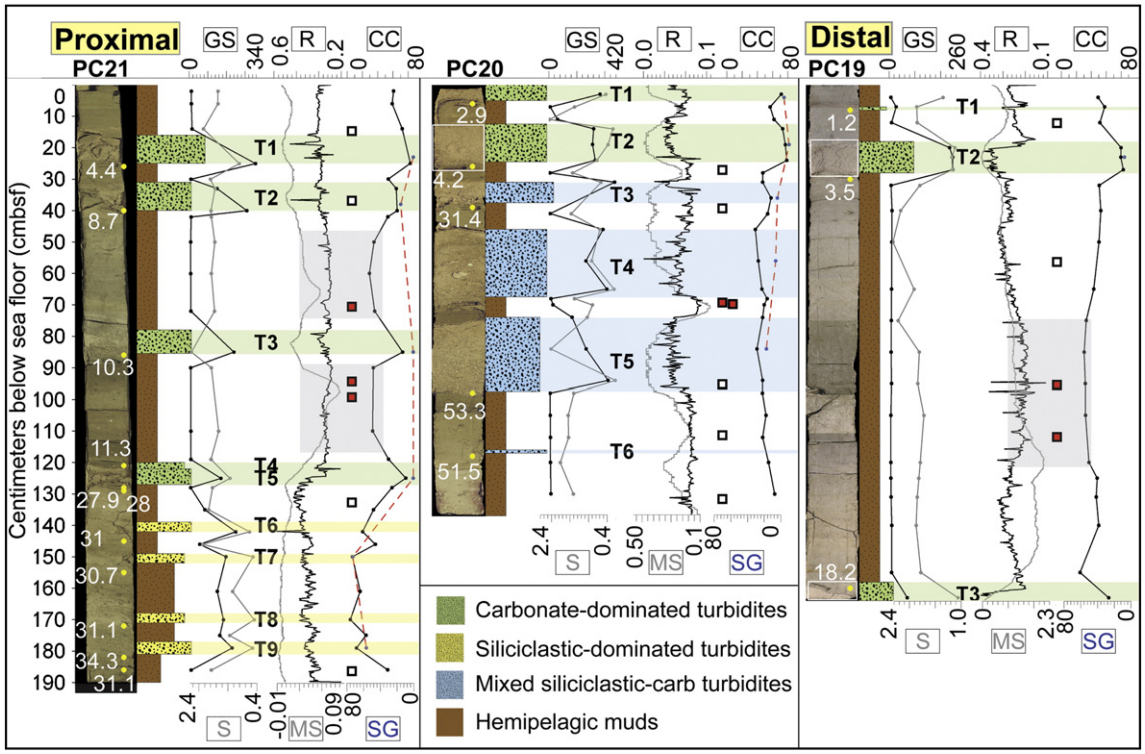

Fig. 4. Ribbon Reef canyon core data showing core logs, images, grain size (GS μm), sorting (S phi), magnetic susceptibility (MS 10^{-4} SI), reflectance (R nm), $CaCO_3$ content (CC %), siliciclastic grains (SG %) and calibrated AMS-C14 ages (white text in ka). Vertical gray rectangles indicate intervals in the hemipelagic muds in PC21 and PC19 that correspond to the late transgressive period that are characterized by low $CaCO_3$ contents, darkest color reflectance, and characteristic highs in both MS and mangrove pollen contents (red-filled square symbols; see Fig. 8 for all pollen data). White boxes in the PC20 and PC19 core images show the location of representative X-radiograph images of the turbidites (see Figs. 6 and 7).

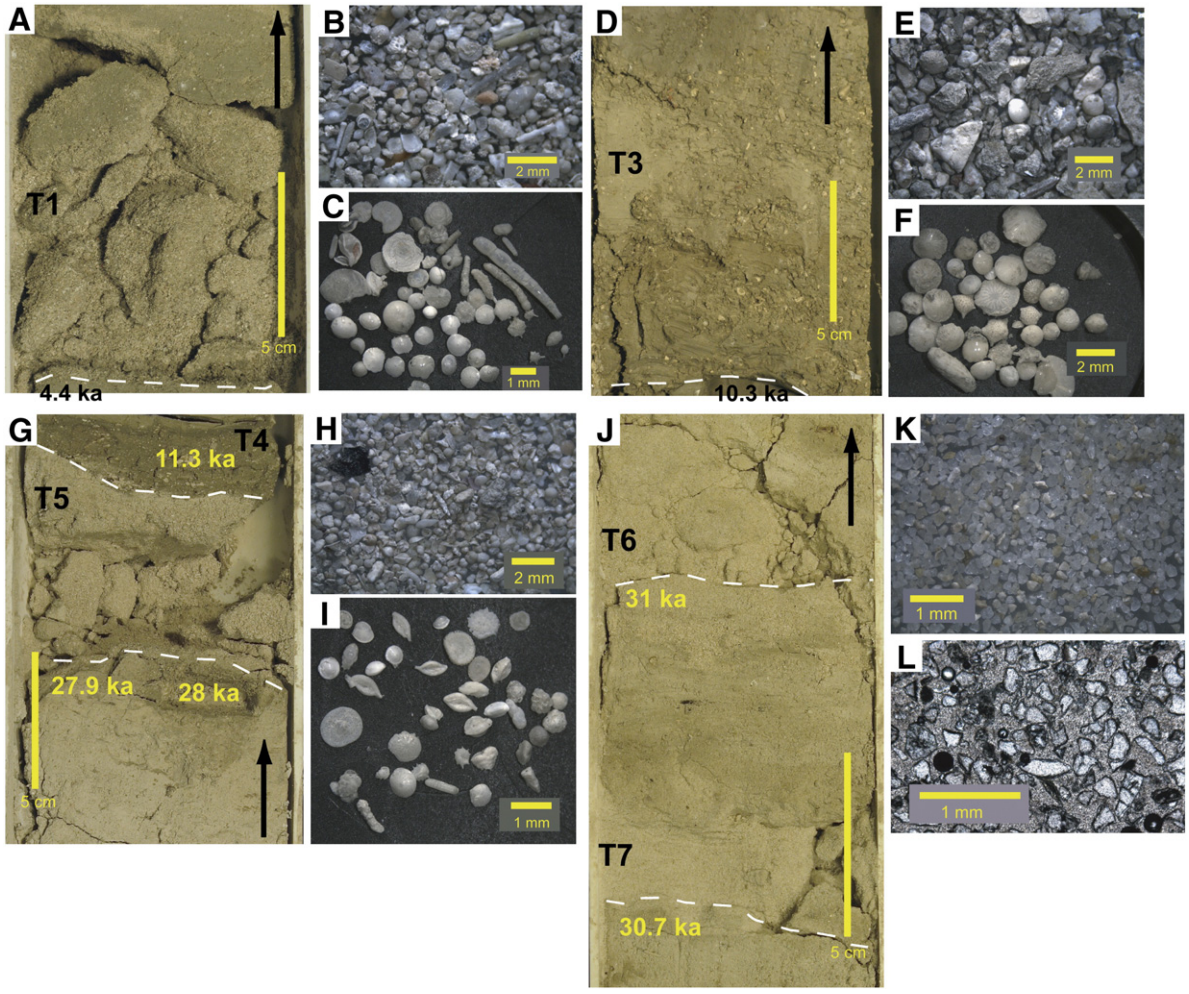

Fig. 5. Close up images of the PC21 turbidite deposits. A: Carbonate-dominated turbidite deposit T1: B–C: Binocular microscope images of the coarse (>250 μm) sediment composition and benthic foraminifera assemblages. D: Carbonate-dominated debrite deposit T3. Note the coarse carbonate grains floating within the brown muddy matrix. E–F: Microscope images of the coarse sediment composition and benthic foraminifera assemblages. G: Carbonate-dominated debrite (T4) and turbidite deposit (T5). H–I: Microscope images of the coarse sediment composition and benthic foraminifera assemblages. J: Siliciclastic-dominated turbidite deposits T6 and T7. K–L: Binocular and thin section images of the mainly well-sorted, fine-grained quartz sands.

carbonate content, we classified the turbidites as: (1) siliciclastic-dominated (<40% $CaCO_3$); (2) carbonate-dominated ("calci-turbidites") (>60% $CaCO_3$); and (3) mixed siliciclastic/carbonate (40–60% $CaCO_3$). Sediment sources were also assessed using magnetic susceptibility, color reflectance and grain composition data. We also investigated the composition of the inter-bedded, mainly hemipelagic sediments in a similar fashion, including analysis of their pollen content.

The most proximal cores (PC21, 20) record a major shift from siliciclastic-dominated or mixed turbidites, to carbonate-dominated turbidites towards the top of the cores (Fig. 4). The lower section of PC21 is characterized by four, siliciclastic-dominated turbidites (T9–T6), composed of moderately well sorted, fine- to medium-grained sands with carbonate contents ranging from 4 to 22%. These turbidites are dominated by well-rounded to subrounded clear quartz grains and minor woody fragments consistent with a terrestrial source (Fig. 5J–L). Previous SEM analysis by Blakeway (1991) indicates the quartz grains are characteristic of aeolian grains, likely sourced originally from the silica rich coastal sand dunes and catchments south of Cape Flattery (Fig. 1) (Lambeck and Woolfe, 2000). A sharp transition is observed at 127 cmbsf with significant increases in the magnetic susceptibility, color reflectance, mud carbonate contents and a switch to carbonate-dominated turbidites (Fig. 5G). Four carbonate-dominated turbidites are recognized (T5–T1) with carbonate contents ranging 70–83%. T4 and T3, between 122 and 78 cmbsf, are different texturally — very poorly-sorted due to their abundant muddy matrix and better classified as debrites commonly associated with debris flows and related mass-failures (Piper et al., 1985; Amy et al., 2005) (Fig. 5D). PC20 records a similar depositional pattern, but in this case there is a shift from four mixed siliciclastic-carbonate turbidites (T6–T3) (Fig. 6D–N) to two carbonate-dominated turbidites (T2–T1) at the top of the core (Fig. 6A). In contrast, only three thin, fine-grained (silt-fine sand) carbonate-dominated turbidites (T3–T1) characterize PC19 (Fig. 7A–E).

All three cores also show a general trend within hemipelagic muds of increasing carbonate content up core, with highest values (60–68%) towards the core tops (Fig. 4). Closer examination of the middle sections of PC21 and PC19 shows a distinct dark grayish section of hemipelagic mud between 115–45 cm and 125–75 cm respectively. These intervals (vertical gray rectangles in Fig. 4) record consistently low carbonate contents (38–31%), dark color reflectance, and characteristic highs in the magnetic susceptibility values. Palynological data confirm that these intervals record the highest counts of *Ceriops*/*Brugiera* and *Rhizophora* pollen, consistent with a strong mangrove signature (Grindrod et al., 1999) (Figs. 4, 8).

Compositional analysis of the coarse (>250 μm) carbonate fractions of each turbidite and debrite shows that, regardless of their carbonate content, they are mainly sourced from neritic environments. Identifiable grains consist mainly of larger benthic foraminifera with

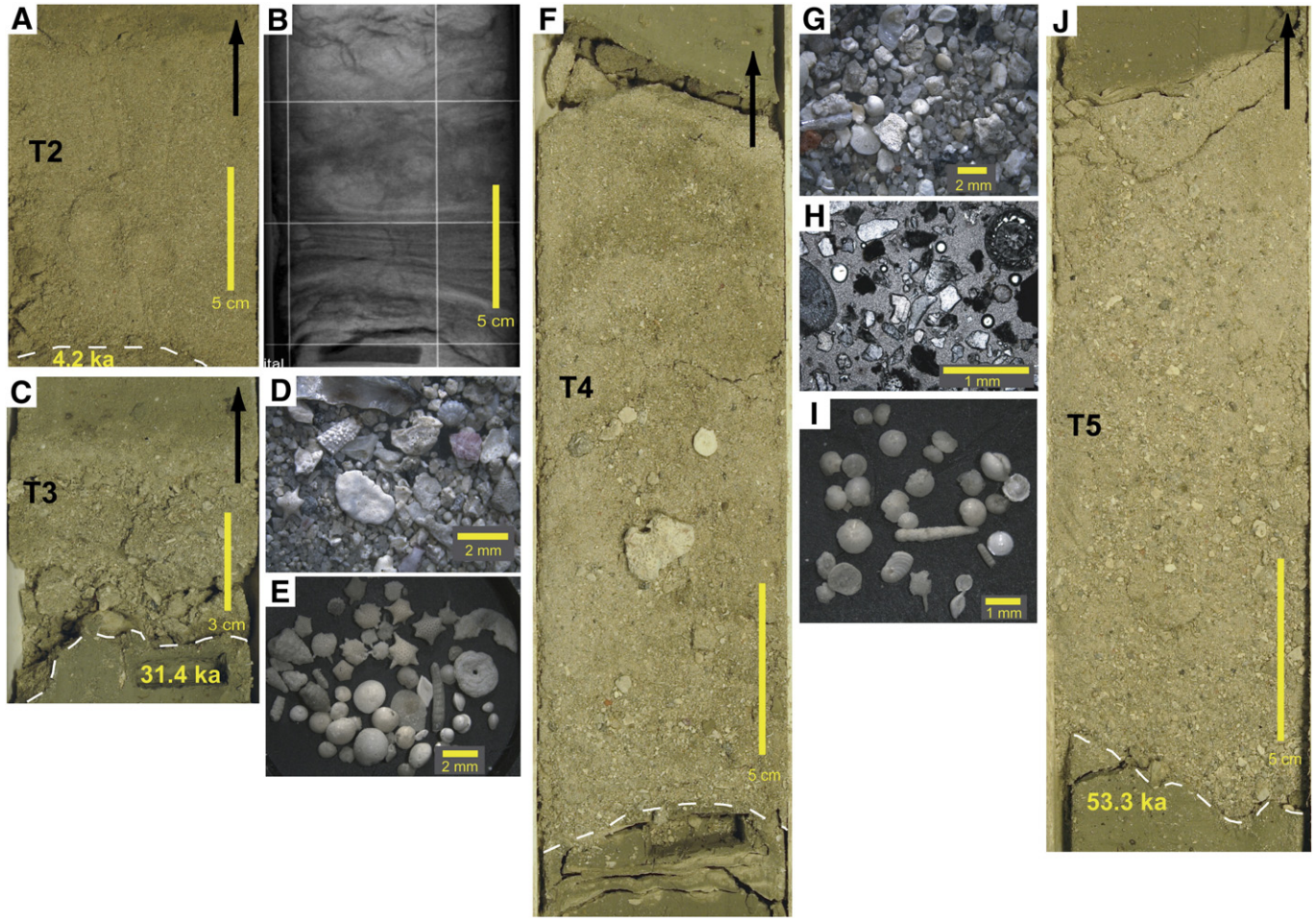

Fig. 6. Close-up images of the PC20 turbidite deposits. A: Carbonate-dominated turbidite deposit T2. B: X-radiograph image showing the erosive turbidite base and parallel laminations. C: Carbonate-dominated turbidite deposit T3. Note the very course-grained turbidite base and sharp, erosive contact with the underlying hemipelagic mud. D–E: Microscope images of the coarse-grained sediment composition and benthic foraminifera assemblage. F: Mixed siliciclastic-carbonate turbidite deposit T4. G–I: Microscope and thin section images of the coarse-grained (>250 μm) composition (including quartz grains) and benthic foraminifera assemblage. Note the abundant sub-rounded clear quartz grains and cm-sized coral fragments. J. Mixed siliciclastic-carbonate turbidite deposit T5. Note the sharp, erosive contact with underlying hemipelagic mud.

minor, sometimes cm-sized, coral, coralline algal, mollusk and echinoid fragments (e.g. PC20 T4; Fig. 6G). The abundance and composition of larger benthic foraminifera (*Baculogypsina*, *Marginopora*, and *Calcarina* cf *hispida*) is typical of very shallow, reef flat settings (<5 m) (Renema, 2006). Also present are reef slope (*Heterostegina depressa*, *Amphistegina lessonii*, *Calcarina mayori*) and inter-reef species (*Operculina*, *Alveolinella*, *Elphidium* sp.). The co-occurrence of abundant planktonic foraminfera (e.g. *Globigerinoides ruber*), pteropods and small non-photosynthetic benthic foraminifera (*Uvigerina*, *Ehrenbergina*, and *Textularia*) in the turbidites, also indicates the entrainment and mixing of material from deeper upper-slope environments during movement through the canyon system. This pattern of mixed planktonic and neritic bioclasts was also observed in turbidites deposited on the slope and basin further south in ODP Sites 821 and 823 respectively (Montaggioni and Venec-Peyré, 1993; Watts et al., 1993).

3.3. Turbidite depositional age

The 20 calibrated radiocarbon ages range from 53 to 1.2 ka (Fig. 4, Table. 1). The two oldest ages in PC20, however, likely represent "background" ages older than about 50 ka. In PC21 the four lower siliciclastic-dominated turbidites (T9–T6) were deposited between 34.4 ka and 30.7 ka. Two ages confirm that the depositional shift to carbonate-dominated turbidites and debrites occurs after ~28 ka (T5) and continues with events after ~11.3 ka, 10.3 ka, 8.7 ka and 4.4 ka. This ages and the lack of hemipelagic deposits, may indicate a hiatus or erosive event following the deposition of T5. In PC20 the mixed siliciclastic-carbonate turbidites were deposited between >50 ka and 34 ka and the shift to carbonate-dominated turbidites up core occurs after 4.2 ka with a second event at 2.9 ka. PC20 may also record a significant hiatus between T3 and T4 (Fig. 4), but this pattern of late Holocene carbonate-dominated turbidites at the top of the core is also observed in PC19 with similar deposits after 3.5 ka and 1.2 ka. The age of T3 (18.2 ka) is poorly constrained because it comes from above the turbidite at the base of PC19. At best this could indicate turbidite deposition prior 18.2 ka, and at worst this age could be biased (i.e. towards older) if any part of the turbidite "tail" had been sampled inadvertently. Finally, the age data confirm that the observed peak in the siliciclastic and mangrove pollen content of the hemipelagic muds in the middle sections of PC21 and PC19 likely corresponds to the late transgressive period, similar to the pattern observed in cores from the inter-canyon areas in the region (Dunbar and Dickens, 2003; Page et al., 2003; e.g. PC27A, PC22), and upper slope further south (Grindrod et al., 1999; e.g. ODP Site 820; Dunbar and Dickens, 2003). This transgressive mud section appears to be absent from PC20 (Fig. 4), either not deposited, or more likely eroded away given the location of this core in the channel axis and within a sandwave field (Fig. 3).

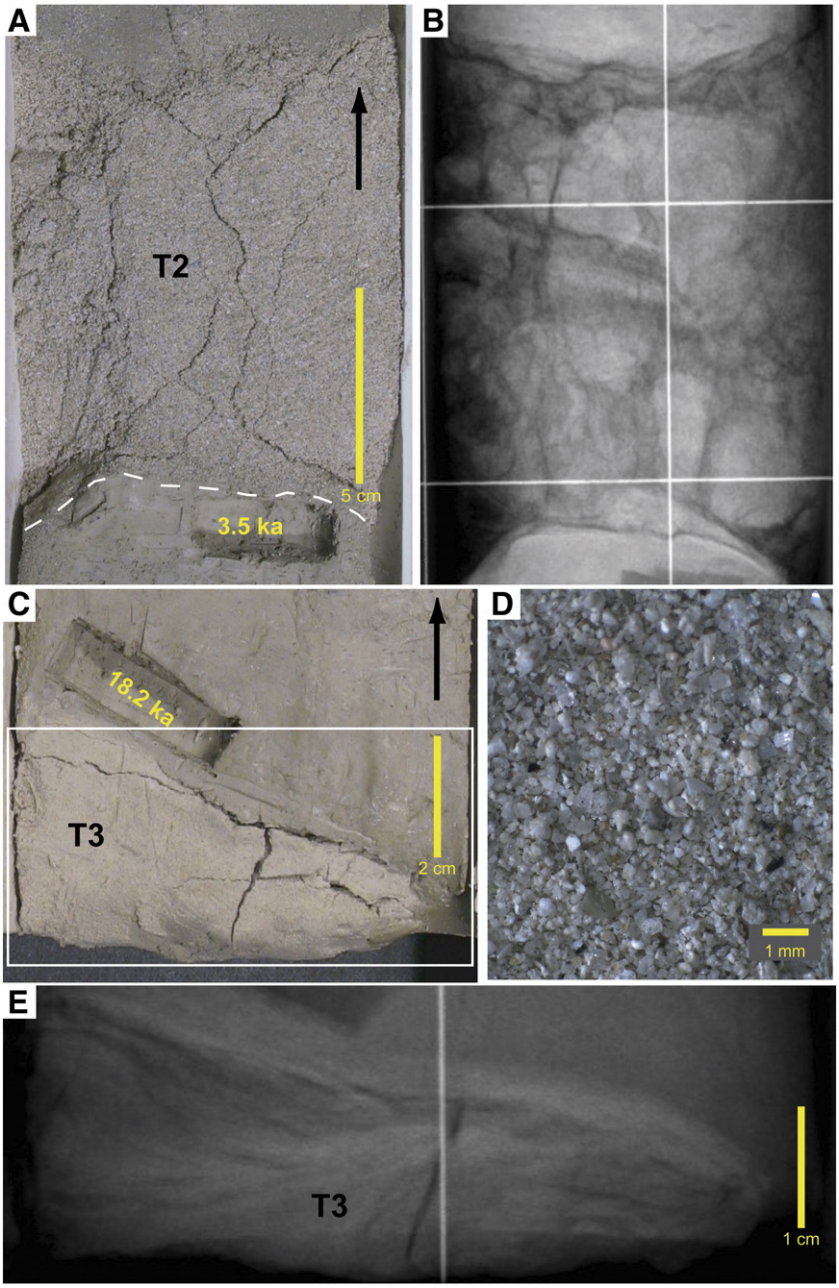

Fig. 7. Close-up images of the PC19 turbidite deposits. A: Carbonate-dominated deposit T2. B: X-radiograph image showing the sharp erosive base and structure-less turbidite deposit. C: Photograph of the carbonate-dominated turbidite deposit T3. D: Microscope images showing the coarse sediment composition. E: X-radiograph image showing a close up of T3 characterized by fine cross laminations.

4. Discussion

The history of canyon activity, turbidite deposition and relationship to sea level change since the Late Pleistocene is summarized in Figs. 9 and 10. Our data define a complex and active canyon system that we broadly interpret in the context of changing siliciclastic and carbonate sediment sources, local reef and shelf morphology, and their relationship to millennial-scale eustatic sea level variability. Critically, we find that the deposition of siliciclastic-dominated and mixed turbidites occurred prior to about 31 ka during MIS3, and apparently not recorded during the full lowstand of MIS2, which the traditional *reciprocal* model would predict. Nor does it occur during the early transgression of MIS1 that the more recent *transgressive shedding* model might predict, if the same processes responsible for the observed influx of fine siliciclastics, were also responsible for the delivery of coarse siliciclastic sediments to the canyons.

4.1. Siliciclastic turbidite deposition during MIS3

Precise constraints are still controversial (Siddall et al., 2008), but several robust sea level reconstructions (e.g. Thompson and Goldstein, 2006) show that MIS3 sea level oscillated about 20–50 m on millennial time scales (7–10 ka) between 50 and 100 m below present sea level as it fell towards MIS2 (Fig. 9) at 120–130 m. Globally these sea level variations have also been associated with Daansgard–Oeschger (D–O) climate cycles and massive ice-discharges,

Table 1
Ribbon Reef canyon core AMS-C14 data.

Core number	Lat (°S)	Long (°E)	Depth (m)	Canyon context	Core length (cm)	Core recovery (%)	Turbidite (%)	Sample number	Lab ID[a]	Sample depth (cmbsf)	Sample context	Radiocarbon ages (^{14}C yrs BP)	^{14}C yrs BP error	Calibrated ages (ka)	2σ age range (ka)	Turbidite event #
FR5/90 PC21	−15.0217	145.8300	−1982	Proximal	190	68	25.8	90/21_1	OZJ840	26	Hemipelagic mud below T1	4280	50	4.38	4.22–4.52	T1
								90/21_4	OZJ841	40	Hemipelagic mud below T2	8170	160	8.68	8.32–9.09	T2
								90/21_7	OZJ842	86	Hemipelagic mud below T3	9480	100	10.33	10.14–10.54	T3[b]
								90/21_17	OZL174	121	Hemipelagic mud within T4	10310	70	11.30	11.16–11.45	T4[b]
								90/21_9	OZJ843	128	Hemipelagic mud below T5	23460	230	27.86	27.42–28.46	T5
								90/21_21	OZL175	129	Hemipelagic mud below T5	23600	140	28.04	27.68–28.49	T5
								90/21_13	OZL170	145	Hemipelagic mud below T6	26680	180	30.95	30.58–31.20	T6
								90/21_14	UBA-10554	155	Hemipelagic mud below T7	26358	84	30.73	30.44–31.01	T7
								90/21_15	OZL172	172	Hemipelagic mud below T8	26950	180	31.11	30.86–31.32	T8
								90/21_16	OZL173	182	Hemipelagic mud below T9	30060	240	34.30	33.54–34.79	T9
								90/21_22	OZL176	186	Hemipelagic mud 5 cm below T9	27020	250	31.13	30.77–31.42	T9
FR5/90 PC20	−15.0517	145.8700	−2110	Mid	137	48	50.7	90/20_2	OZJ837	6	Hemipelagic mud below T1	3130	70	2.90	2.74–3.10	T1
								90/20_5	OZJ838	25.5	Hemipelagic mud below T2	2945	40	2.72	2.59–2.82	T2
								90/20_5A	UBA-10555	26	Hemipelagic mud below T2	4164	25	4.22	4.12–4.35	T2
								90/20_8	OZJ839	39	Hemipelagic mud below T3	27580	280	31.40	31.07–31.90	T3
								90/20_12	OZL169	98	Hemipelagic mud below T5	49300	1500	53.34	50.57–56.11	T5
								90/20_19	OZL171	118	Hemipelagic mud below T6	48000	1300	51.47	49.06–53.87	T6
FR5/90 PC19	−15.1067	145.9133	−2220	Distal	164	68	9.8	90/19_18	UBA-10556	8	Hemipelagic mud below T1	1637	25	1.19	1.11–1.27	T1
								90/19_3	OZJ835	30	Hemipelagic mud below T2	3580	50	3.46	3.34–3.59	T2
								90/19_6	OZJ836	160	Hemipelagic mud above T3	15310	160	18.17	17.71–18.56	T3

[a] OZJ# & OZL# AMS-C14 analyses were measured at Australian Nuclear Science and Technology Organisation (ANSTO); UBA-# AMS-C14 analyses were measured at the 14CHRONO Centre, Queens University Belfast.
[b] Based on their sedimentary characteristics (see text and Fig. 5 for details) these deposits are interpreted as debrites (Amy et al., 2005).

Table 2
Summary of sedimentary data for the turbidites in the Ribbon Reef canyon cores.

Core number	Turbidite event #	Depth (cm)	Thickness (cm)	Stratigraphic notes	Sediment texture								Sediment composition		
					Grain size (um)		Sorting (phi)		Skewness (phi)		Kurtosis (phi)		Carbonate content (%)	Bioclastic grain components	Summary
FR5/90 PC21	T1	16–25	9	Erosive base	356	Medium sand	0.98	Moderately sorted	−0.21	Coarse	1.21	Leptokurtic	89.5	Mixed deep and shallow	Carbonate-dominated
	T2	31–40	9	Erosive contact, graded, planar lamination at base	229	Medium–fine sand	1.88	Poorly sorted	−0.42	Strongly course	1.74	Very leptokurtic	70.2	Mixed deep and shallow	Carbonate-dominated
	T3[a]	78–85	11		240	Fine sand and mud matrix	2.62	Very poorly sorted	−0.65	Strongly coarse	1.03	Mesokurtic	78.4	Mixed deep and shallow	Carbonate-dominated
	T4[a]	120–122	2	Erosive base		Mud matrix									Carbonate-dominated?
	T5	122–127	5	Erosive base	171	Fine sand	1.30	Poorly sorted	−0.30	Coarse	1.54	Very leptokurtic	83.06	Mixed deep and shallow	Carbonate-dominated
	T6	139–142	3	Erosive base	250	Medium sand	0.63	Moderately well sorted	−0.03	Near symmetrical	0.92	Mesokurtic	22.1	Mixed deep and shallow	Siliciclastic-dominated
	T7	149–152	3	Erosive base	198	Fine sand	0.51	Moderately well sorted	−0.01	Near symmetrical	0.94	Mesokurtic	7.6	Mixed deep and shallow	Siliciclastic-dominated
	T8	168–171	3	Erosive base	184	Fine sand	0.47	Well sorted	0.00	Near symmetrical	0.96	Mesokurtic	4.6	Mixed deep and shallow	Siliciclastic-dominated
	T9	177–181	4	Erosive base	230	Fine sand	0.53	Moderately well sorted	−0.01	Near symmetrical	0.94	Mesokurtic	13.0	Mixed deep and shallow	Siliciclastic-dominated
FR5/90 PC20	T1	0–5	5	Erosive base	366	Medium sand	0.97	Moderately sorted	−0.18	Coarse	1.18	Leptokurtic	77.1	Mixed deep and shallow	Carbonate-dominated
	T2	12.5–24.5	12	Erosive base	321	Medium sand	0.96	Poorly–moderately sorted	−0.22	Strongly coarse-coarse	1.34	Leptokurtic	82.2	Mixed deep and shallow	Carbonate-dominated
	T3	31–37.5	7	Erosive base	470	Medium sand	1.10	Poorly sorted	−0.25	Coarse	1.01	Mesokurtic	56.6	Mixed deep and shallow	Mixed siliciclastic-carbonate
	T4	46–67.5	22	Erosive base	356	Medium sand	1.07	Poorly sorted	−0.26	Coarse-strongly coarse	1.51	Mesokurtic–very leptokurtic	44.8	Mixed deep and shallow	Mixed siliciclastic-carbonate
	T5	74–97.5	24	Erosive base	286	Medium–fine sand	1.10	Moderately–poorly sorted	−0.15	Near symmetrical-coarse	1.11	Mesokurtic-leptokurtic	47.9	Mixed deep and shallow	Mixed siliciclastic-carbonate
	T6	116–117	1			Coarse gravel and mud matrix		Very poorly sorted							Mixed siliciclastic-carbonate
FR5/90 PC19	T1	7–8	1	Thin silt layer	27	silt	1.82	Poorly sorted	−0.36	Strongly coarse	1.10	Mesokurtic	60.9		Carbonate-dominated
	T2	18–28	10	Sharp, eroded base	243	Fine sand	1.11	Poorly sorted	−0.22	Coarse	1.35	Leptokurtic	85.1	Mixed deep and shallow	Carbonate-dominated
	T3	158–163	5	Cross laminations	71	Very fine sand	1.02	Poorly sorted	−0.19	Coarse	1.24	Leptokurtic	66.7		Carbonate-dominated

[a] Based on their sedimentary characteristics (see text and Fig. 5 for details) these deposits are interpreted as debrites (Amy et al., 2005).

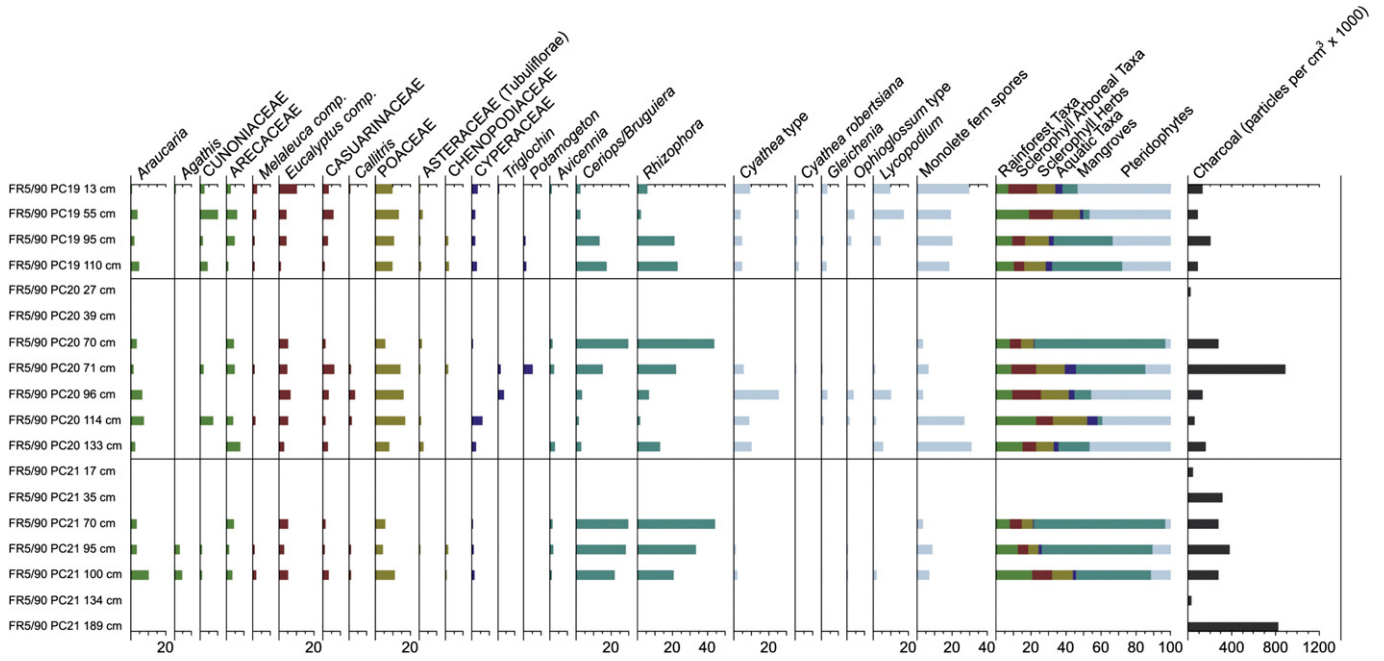

Fig. 8. Selected features of the palynological record of the FR5/90 PC19, PC20 and PC21 cores. All pollen values are expressed as percentages of the total pollen sum for the appropriate sample.

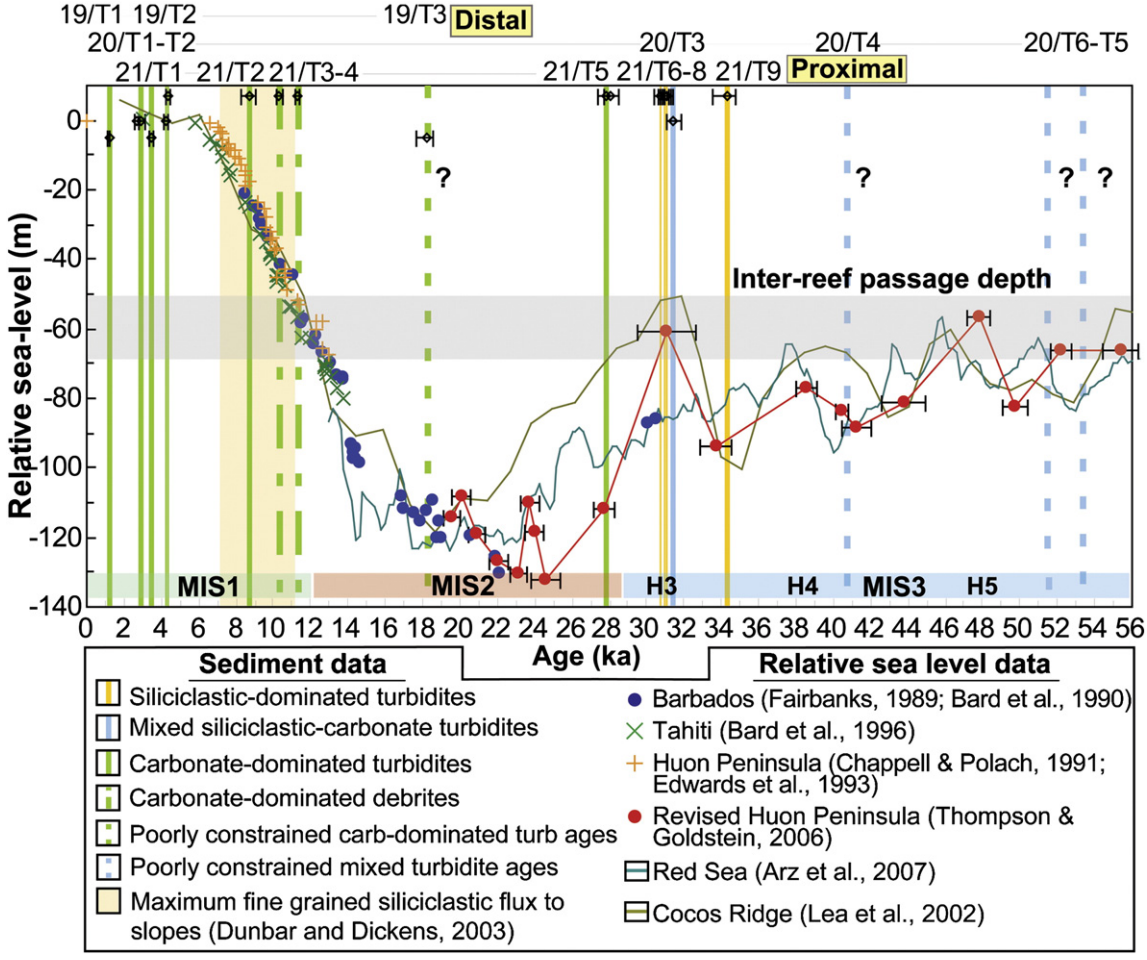

Fig. 9. Relationship between turbidite composition, depositional timing, inter-reef passage depth (horizontal gray bar) and Late Pleistocene sea level change. Calibrated radiocarbon turbidite ages are plotted against different relative sea level records (corals — Barbados, Tahiti, Huon Peninsula; sediments — Red Sea, Cocos Ridge). Marine isotope stages (MIS3-1) and Heinrich events (H5-3) are also shown. The period of maximum flux of fine-grained, hemipelagic siliciclastic sediments to the slope and basin of the northern GBR margin is represented by the vertical yellow bar between ~7–11 ka (Dunbar and Dickens, 2003).

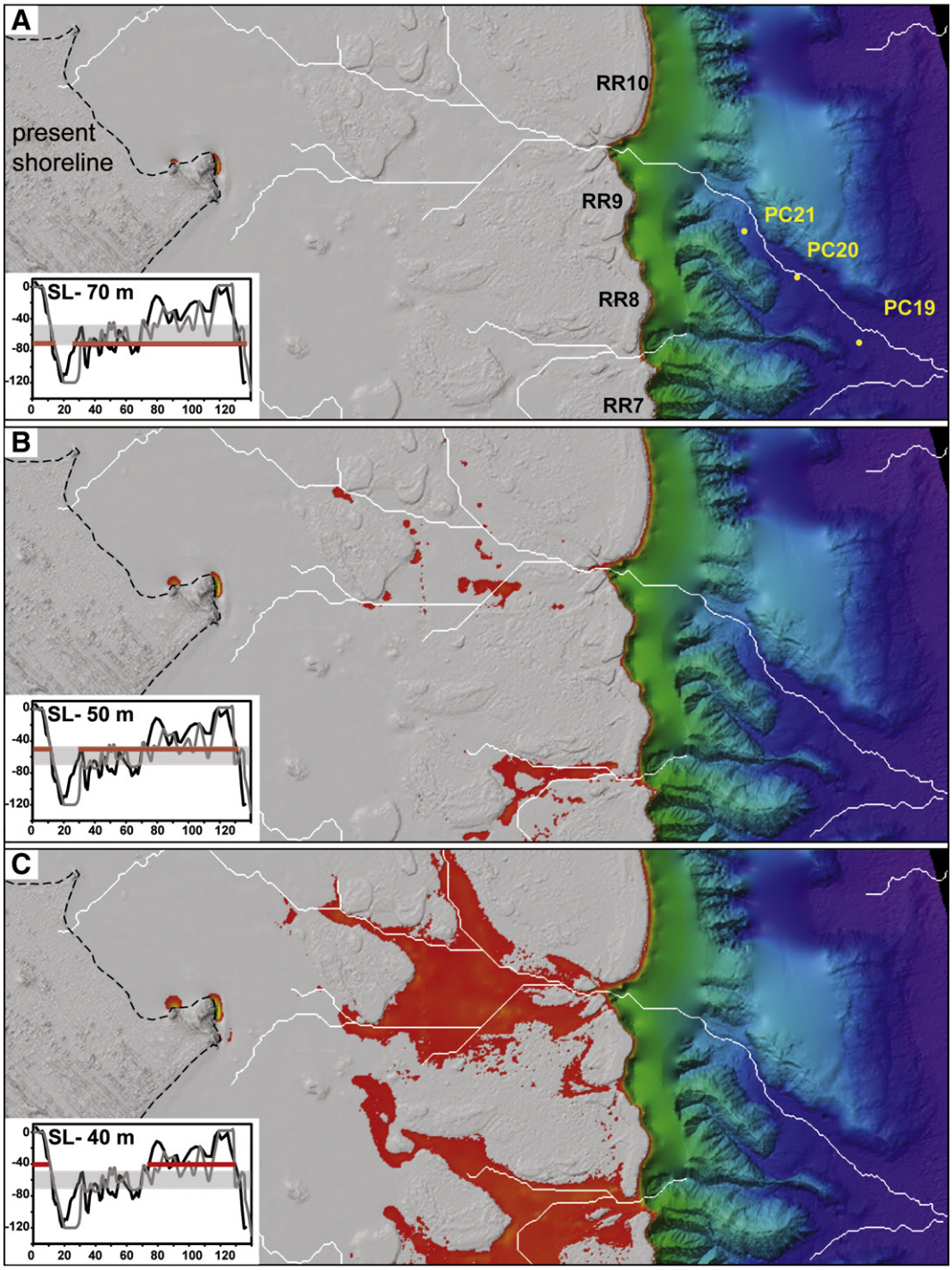

Fig. 10. Relationship between sea level change, the inter-reef passage depth (horizontal gray bar) and shelf inundation (red line and colored hillshading). A: Sea level position at −70 m, while close to the shelf break, does not breach most of the inter-reef passages. B: Sea level position at −50 m clearly breaches the inter-reef passages and inundates the deeper reaches of the shelf. C: Sea level at −40 m inundates at least one third of the shelf. The insets showing Quaternary sea level is after Lea et al. (2002) (black line) and Lambeck and Chappell (2001) (gray line).

known as Heinrich (H) events (Siddall et al., 2008). Several workers (Woolfe et al., 1998; Dunbar et al., 2000; Page et al., 2003) have speculated that during lower sea levels siliciclastic sediments were ponded on the GBR outer-shelf behind the carbonate highs provided by the exposed MIS5e (125 ka) reefs (International Consortium, G.B.R.D., 2001). While a direct connection between the newly imaged cross-shelf paleo-channel system (Fig. 2), inter-reef passages and canyon system is difficult to establish, we suggest this system could have acted as a conduit for coarse siliciclastic sediments (Fig. 1), at least during times when sea level repeatedly intersected the inter-reef passages (Figs. 9, 10).

A recent investigation (Francis et al., 2007) of surficial sediments found that some inter-reef passages further south offshore from Cooktown and Cairns, have higher siliciclastic contents (up to 60%) than the adjacent outer-shelf. This pattern could have been enhanced during lower sea levels due to the closer proximity of siliciclastic sediment sources and reduced shallow carbonate production. Regardless of exactly how or when the coarse siliciclastic sediments were deposited on the outer shelf, we suggest that the prolonged period (>25 ka) of MIS3 sea level oscillations would have repeatedly intersected the inter-reef passages and adjacent areas on the shelf that

lie between 50 and 70 m (Figs. 9, 10B, C). This may have caused significant re-mobilization and mixing via waves and tidal currents of any locally-stored coarse siliciclastic (and carbonate sediments), allowing subsequent transport to Canyon 1 via sediment gravity flows.

Also noteworthy is the peak of siliciclastic-dominated turbidite deposition observed in the proximal PC21 towards the end of MIS3 (34–31 ka), and their apparent absence after this time. Precise constraints on eustatic sea levels during the transition from MIS3 and MIS2 are difficult (Siddall et al., 2008). However, relative local sea level data (Lea et al., 2002; Thompson and Goldstein, 2006) show that sea level fell, albeit briefly, to its lowest base level (90–100 m) during MIS3 just prior to a significant rise to 50–60 m associated with the H3 event, before falling dramatically to MIS2 (Figs. 9, 10A). This could have caused the fluvial/coastal system to prograde further out, or more likely, given the rate fall, the system to be abandoned completely (i.e. no longer connected to the canyon head, Fig. 9A) allowing aggradation and sediment infilling (Woolfe et al., 1998). In either case, any remaining coarse-grained siliciclastic sediments stored in, or adjacent to, the inter-reef passages, could have been subsequently re-mobilized during the H3 rise before the shelf was finally and completely abandoned during the MIS2 lowstand. Recent high-resolution chronologic investigations (Jorry et al., 2008; Lebreiro et al., 2009) of other submarine canyons have also reported increases in turbidite deposition forced by millennial-scale sea level variations, particularly during rapid sea level rise causing sediment instability and/or rapid switching on and off of sediment factories.

4.2. Lack of turbidites during the MIS2 sea level lowstand?

Perhaps the most striking depositional pattern in the Ribbon Reef canyon cores is the apparent lack of mixed or siliciclastic turbidites during the lowstand (120–130 m) of MIS2. This pattern is not consistent with the *reciprocal* model nor previous estimates of the timing of turbidite deposition further south in the GBR (Watts et al., 1993; Dunbar et al., 2000; Page et al., 2003). Similar to the *transgressive shedding* model explaining the lack of siliciclastic flux during this MIS2 period, the Ribbon Reef canyon record suggests any available coarse siliciclastic sediments, abundant during MIS3, were indeed trapped behind the now fully exposed and disconnected shelf edge. That said, we cannot completely discount the lack of siliciclastic turbidites at this time because: (1) the reduced precipitation regime during MIS2 (Williams et al., 2009) may also have reduced siliciclastic supply; (2) they could have been bypassed and deposited further down the canyon axis and basin and not recorded in the cores as was proposed by Peerdeman and Davies (1993) and/or (3) they could have been eroded away by subsequent turbidite events or local landslides which are observed in the bathymetry data (Fig. 3). However, based on their analysis of the GLORIA sidescan data, Dunbar et al. (2000) argued that the lack of any large fan complexes on the lower slope is not consistent with this bypass process nor does this account for the high accumulation of fine siliciclastic sediments during the late transgression (Dunbar et al., 2000). Our age data confirm that carbonate-dominated turbidites were deposited between 28 ka and 18 ka (MIS2) but we cannot confirm that significant portions of the turbidite record have not been removed by erosion, particularly in the two proximal cores (PC21, 20). However, if we assume no significant hiatus the presence of only a few carbonate-dominated turbidites during this MIS2 period could be explained by sediments sourced directly from the fossil shelf edge reefs preserved between 50 and 100 m Ribbon Reef (Expedition 325 Scientists, 2010; Yokoyama et al., 2011). Finally, whether the well-developed Ribbon Reefs were able to "block" or trap the passage of coarse siliciclastics (and most carbonates) during the lowstand remains an intriguing question. For example, unlike the Ribbon Reef cores, Page et al. (2003) noted the presence of thin siliciclastic sandy turbidites during the early transgression. Further, Dunbar et al. (2000) observed increased turbidite frequency during the lowstand but little information was provided about the turbidite compositions nor was their timing constrained by direct age determinations. One possible explanation is that the much wider, open and deeper shelf and shelf edge off Cairns (Beaman et al., 2008; Abbey et al., 2011) could have allowed more "leakage" of coarse siliciclastic sediments stored on the shelf at lower sea level positions. This idea remains to be tested by more direct and precise dating of the turbidite activity across this wider region.

4.3. Carbonate turbidite shedding and fine siliciclastic flux during the MIS1

Few turbidites occur during the early to mid transgression (19–12 ka), but carbonate-dominated turbidite sedimentation is well established from the late transgression ~11 ka, and continues through MIS 1 until as recently as 1.2 ka (Fig. 4). The presence of coarse carbonate sediments at the top of PC20 (T1) and its location in the sandwaves in the channel axis confirms the recent and likely on-going canyon activity (e.g. Paull et al., 2010; Wynn and Stow, 2002; Xu et al., 2008). Minor siliciclastic sediments occur in these turbidites but the high carbonate contents are derived mainly from shallow coral reef sources. This reflects the turn-on and dominance of shallow-water (neritic) carbonate production during the flooding of the shelf about 11–10 ka when sea level was 50 to 40 m (Fig. 10B, C), followed by continued flooding and the westward retreat of the coastline during MIS1. In the Ribbon Reef region, this likely reflected the turn-on first of the *Halimeda* deposits (11–10 ka) (Marshall and Davies, 1988) on the shelf, followed by the Ribbon Reefs themselves (9–8 ka) (Davies et al., 1985; International Consortium, G.B.R.D., 2001). This finding is consistent with the classical highstand shedding (Schlager et al., 1994) of the *reciprocal* model, and the *transgressive shedding* model, which also shows high rates of fine-grained carbonate accumulation on the slope at these times (Page et al., 2003).

Interestingly, the canyon cores (PC21, PC19) outside of the main channel axis also record a dark and siliciclastic-rich horizon within the transgressive interval (~11–8 ka) of the hemipelagic muds (Fig. 4), consistent with that observed in the inter-canyon cores (Dunbar and Dickens, 2003). Our new palynologic data (Figs. 4, 8) also confirm the Ribbon Reef canyon cores clearly record a strong mangrove signature within these horizons, indicating well-developed mangrove communities on the adjacent shelf during this period. This provides strong independent support for the *transgressive shedding* model and the idea that the fine siliciclastics may have come from a marginal marine rather than direct riverine sediment source (Grindrod et al., 1999; Dunbar and Dickens, 2003). In the context of the pattern of turbidite sedimentation in the cores this has several important implications. First, it suggests that turbidite sedimentation in the canyons is generally superimposed on the regional *transgressive shedding* pattern of hemiplegic sedimentation. Second, the complete lack of siliciclastic turbidites in the late transgression, also the period of maximum flux of fine siliciclastics, requires further investigation as it implies that coarse siliciclastic sources to these canyons were at this time: (1) either already depleted during the prolonged and repeated MIS3 sea level instability and dominant siliciclastic turbidite deposition; (2) if available, then not able to be mobilized by the same sedimentary processes responsible for the huge influx of fine siliciclastic sediments; and/or (3) completely overwhelmed by the volume of coarse carbonate sediments from the now productive shallow carbonate factory.

4.4. Limitations and future work

We stress that our reconstruction of turbidite sedimentation comes from one canyon system so whether it is representative of the entire Ribbon Reef region, let alone the entire GBR margin, remains an open question. Questions also remain about causes of possible hiatuses in

the turbidite record, which can only be solved by more systematic and dense coring of different parts of the same canyon system (i.e. channel vs. levee; proximal vs. distal). However, our data do provide important new insights into how reef and shelf morphology, acting in combination with millennial-scale sea level oscillations, can influence turbidite deposition in mixed tropical systems on a rimmed margin (Jorry et al., 2008). Future studies will focus on other cores from other canyons along the GBR margin in order to develop a complete depositional model that accounts for both hemipelagic and turbidite sedimentation, their relative carbonate and siliciclastic contributions, and how this varies in space and time.

5. Conclusions

Our new data constrain the Late Pleistocene history of turbidite sedimentation in a submarine canyon off the northern GBR and we conclude that:

(1) The composition of the turbidites and debrites reflects the mixed siliciclastic-carbonate system, sourced mainly from the shallow neritic shelf, but also influenced by re-working of material from the deeper slopes.
(2) The chronologic data confirm the canyons have been active since the Late Pleistocene until as recently as the Late Holocene at 1.2 ka. This activity is supported by morphologic evidence showing significant channel development and prominent sandwave features in the canyon axis. Local submarine landslides are possible source of the debrites.
(3) The chronologic and sedimentologic data confirm that the deposition of siliciclastic-dominated and mixed turbidites occurred prior to about 31 ka during MIS3. Our data suggest that siliciclastic-dominated turbidites are absent during the full lowstand of MIS2, inconsistent with the traditional *reciprocal* model, but this could reflect gaps in the turbidite record. Nor do they occur during the early transgression of MIS1, which the *transgressive shedding* model might predict if the same processes responsible for the influx of fine siliciclastics also influenced the delivery of coarse siliciclastic sediments to the canyons.
(4) The prolonged period (>25 ka) of millennial-scale sea level changes during MIS3 favored the influx of coarse siliciclastic sediments in the canyons. Sea level repeatedly intersected the inter-reef passage depth, particularly during the transition to MIS2, allowing either the direct supply, or perhaps more likely the reworking of coarse coastal sediments trapped behind the exposed reef complex. Carbonate-dominated turbidites became fully established following the turn-on of shallow-water (neritic) carbonate production in the early Holocene.
(5) The observed pattern of turbidite sedimentation could represent a model for canyon sedimentation on tropical mixed siliciclastic-carbonate margins, characterized by a well-developed barrier reef system. However, more work is needed on other canyons along the GBR margin to confirm if these patterns are consistent in space and time.

Supplementary materials related to this article can be found online at doi:10.1016/j.palaeo.2012.02.034.

Acknowledgments

This research was funded by the Australian Institute of Nuclear Science and Engineering, James Cook University, Nederlands Centrum voor Biodiversiteit, Leiden, Australian Marine National Facility, National Geographic Society, and the Natural Environment Research Council. APB and RB were supported by postdoctoral fellowships from the Universidad de Granada, Spain and a Smart Futures Fellowship from the Queensland Government respectively. We also thank Gerald Dickens, Gavin Dunbar, Lucien Montaggioni and two anonymous reviewers for their constructive reviews of earlier versions of this manuscript.

References

Abbey, E., Webster, J.M., Beaman, R.J., 2011. Geomorphology of submerged reefs on the shelf edge of the Great Barrier Reef: the influence of oscillating Pleistocene sea-levels. Marine Geology 288, 61–78.
Amy, L.A., Talling, P.J., Peakall, J., Wynn, R.B., 2005. Bed geometry used to test recognition criteria of turbidites and (sandy) debrites. Sedimentary Geology 179, 163–174.
Beaman, R.J., 2010. 3DGBR: a high-resolution depth model for the Great Barrier Reef and Coral Sea. Marine and Tropical Sciences Research Facility (MTSRF) Project 2.5i.1a Final Report, MTSRF, p. 12.
Beaman, R.J., Webster, J.M., Wust, R.A.J., 2008. New evidence for drowned shelf edge reefs in the Great Barrier Reef, Australia. Marine Geology 247, 17–34.
Blakeway, D., 1991. Sedimentary Sources and Processes in Outer Shelf, Slope and Submarine Canyon Environments, Northern Ribbon Reefs, Great Barrier Reef, Australia, School of Earth Sciences. James Cook University, Townsville.
Bostock, H.C., Opdyke, B.N., Gagan, M.K., Fifield, L.K., 2009. Late Quaternary siliciclastic/carbonate sedimentation model for the Capricorn Channel, southern Great Barrier Reef province, Australia. Marine Geology 257, 107–123.
Boyd, R., Ruming, K., Goodwin, I., Sandstrom, M., Schroder-Adams, C., 2008. Highstand transport of coastal sand to the deep ocean: a case study from Fraser Island, southeast Australia. Geology 36, 15–18.
Cantero, M.I., Cantelli, A., Pirmez, C., Balachandar, S., Mohrig, D., Hickson, T.A., Yeh, T.-h., Naruse, H., Parker, G., 2012. Emplacement of massive turbidites linked to extinction of turbulence in turbidity currents. Nature Geoscience 5, 42–45.
Davies, P.J., Marshall, J.F., Hopley, D., 1985. Relationships between reef growth and sea level in the Great Barrier Reef. Proceeding of the Fifth International Coral Reef Congress, Tahiti, pp. 95–103.
Dolan, J.F., 1989. Eustatic and tectonic controls on deposition of hybrid siliciclastic/carbonate basinal cycles: discussion with examples. AAPG Bulletin 73, 1233–1246.
Dunbar, G.B., Dickens, G.R., 2003. Massive siliciclastic discharge to slopes of the Great Barrier Reef Platform during sea-level transgression: constraints from sediment cores between 15[deg]S and 16[deg]S latitude and possible explanations. Sedimentary Geology 162, 141–158.
Dunbar, G.B., Dickens, G.R., Carter, R.M., 2000. Sediment flux across the Great Barrier Reef Shelf to the Queensland Trough over the last 300 ky. Sedimentary Geology 133, 49.
Expedition 325 Scientists, 2010. Great Barrier Reef environmental changes: the last deglacial sea level rise in the South Pacific: offshore drilling northeast Australia. IODP Prel. Rept., 325.
Fielding, C.R., Trueman, J.D., Dickinson, G.R., Page, M., 2003. Anatomy of the buried Burdekin River channel across the Great Barrier Reef shelf: how does a major river operate on a tropical mixed siliciclastic/carbonate margin during sea level lowstand? Sedimentary Geology 157, 291–301.
Folk, R.L., Ward, W.C., 1957. Brazos River Bar: a study in the significance of grain size parameters. Journal of Sedimentary Petrology 27, 3–26.
Francis, J.M., Dunbar, G.B., Dickens, G.R., Sutherland, I.A., Droxler, A.W., 2007. Siliciclastic sediment across the North Queensland Margin (Australia): a Holocene perspective on reciprocal versus coeval deposition in tropical mixed siliciclastic-carbonate systems. Journal of Sedimentary Research 77, 572–586.
Goldfinger, C., Morey, A.E., Nelson, C.H., Gutierrez-Pastor, J., Johnson, J.E., Karabanov, E., Chaytor, J., Eriksson, A., 2007. Rupture lengths and temporal history of significant earthquakes on the offshore and north coast segments of the Northern San Andreas Fault based on turbidite stratigraphy. Earth and Planetary Science Letters 254, 9–27.
Grindrod, J., Moss, P., Kaars, S.V.D., 1999. Late Quaternary cycles of mangrove development and decline on the north Australian continental shelf. Journal of Quaternary Science 14, 465–470.
Hughes-Clarke, J., 1994. Toward remote seafloor classification using the angular response of acoustic backscattering: a case study from multiple overlapping GLORIA data. IEEE Journal of Oceanic Engineering 19, 112–127.
International Consortium, G.B.R.D., 2001. New constraints on the origin of the Australian Great Barrier Reef from an international project of deep coring. Geology 29, 483–486.
Jorry, S.J., Droxler, A.W., Mallarino, G., Dickens, G.R., Bentley, S.J., Beaufort, L., Peterson, L.C., Opdyke, B.N., 2008. Bundled turbidite deposition in the central Pandora Trough (Gulf of Papua) since Last Glacial Maximum: Linking sediment nature and accumulation to sea level fluctuations at millennial timescale. Journal of Geophysical Research 113, F01S19.
Lambeck, K., Chappell, J., 2001. Sea level change through the last glacial cycle. Science 292, 679–686.
Lambeck, A., Woolfe, K.J., 2000. Composition and textural variability along the 10 m isobath, Great Barrier Reef: evidence for pervasive northward sediment transport. Australian Journal of Earth Sciences 47, 327–335.
Lea, D.W., Martin, P.A., Pak, D.K., Spero, H.J., 2002. Reconstruction a 350 ky history of sea-level using planktonic Mg/Ca and oxygen isotope records from a Cocos Ridge core. Quaternary Science Reviews 283, 283–293.
Lebreiro, S.M., Voelker, A.H.L., Vizcaino, A., Abrantes, F.G., Alt-Epping, U., Jung, S., Thouveny, N., Gràcia, E., 2009. Sediment instability on the Portuguese continental

margin under abrupt glacial climate changes (last 60 kyr). Quaternary Science Reviews 28, 3211–3223.
Marshall, J.F., Davies, P.J., 1988. Halimeda biotherms of the northern Great Barrier Reef. Coral Reefs 6, 139–148.
Montaggioni, L.F., Venec-Peyré, M.-T., 1993. Shallow-Water foraminiferal taphocoenoses at Site 821: implications for the Pleistocene evolution of the Central Great Barrier Reef Shelf, Northeast Australia. In: McKenzie, J.A., Davies, P.J., Palmer-Julson, A., et al. (Eds.), Proc. ODP. Sci. Results,. Ocean Drilling Program, College Station, TX, pp. 365–378.
Mount, J.F., 1984. Mixing of siliciclastic and carbonate sediments in shallow shelf environments. Geology 12, 432–435.
Orme, G.R., Salama, M.S., 1988. Form and seismic stratigraphy of Halimeda banks in part of the northern Great Barrier Reef Province. Coral Reefs 6, 131–137.
Page, M.C., Dickens, G.R., Dunbar, G.B., 2003. Tropical view of Quaternary sequence stratigraphy: siliciclastic accumulation on slopes east of the Great Barrier Reef since the last glacial maximum. Geology 31, 1013–1016.
Paull, C.K., Ussler III, W., Caress, D.W., Lundsten, E., Covault, J.A., Maier, K.L., Xu, J., Augenstein, S., 2010. Origins of large crescent-shaped bedforms within the axial channel of Monterey Canyon, offshore California. Geosphere 6, 755–774.
Peerdeman, F.H., Davies, P.J., 1993. sedimentological response of an outer-shelf, upper-slope sequence to rapid changes in Pleistocene eustatic sea level: hole 820A, Northeastern Australian Margin. In: McKenzie, J.A., Davies, P.J., Palmer-Julson, A. (Eds.), Proc.ODP,Sci. Res. Ocean Drilling Program, College Station, Texas, pp. 302–313.
Piper, D.J.W., Farre, J.A., Shor, A., 1985. Late Quaternary slumps and debris flows on the Scotian Slope. Geological Society of America Bulletin 96, 1508–1517.
Posamentier, H.W., Vail, P.R., 1988. Eustatic control on clastic deposition II — sequence and system tracts models. In: Wilgus, C.K., Hastings, B.S., Posamentier, H., Van Wagoner, J., Ross, C.A., Kendall, C.G.St.C. (Eds.), Sea Level Changes: An Integrated Approach. SEPM Special Publication, pp. 125–154.
Puga-Bernabéu, Á., Webster, J.M., Beaman, R.J., Guilbaud, V., 2011. Morphology and controls on the evolution of a mixed carbonate–siliciclastic submarine canyon system, Great Barrier Reef margin, north-eastern Australia. Marine Geology 289, 100–116.
Reimer, P.J., Reimer, R.W., 2010. Marine Radiocarbon Reservoir Correction Database, [WWW Program and Documentation]. 14CHRONO Centre, Queen's University Belfast, Belfast.
Reimer, P.J., Baillie, M.G.L., Bard, E., Bayliss, A., Beck, J.W., Blackwell, P.G., Bronk Ramsey, C., C.B., Burr, G.S., Edwards, R.L., Friedrich, M., Grootes, P.M., Guilderson, T.P., I.H., Heaton, T.J., Hogg, A.G., Hughen, K.A., Kaiser, K.F., Kromer, B., McCormac, F.G., S.M., Reimer, R.W., Richards, D.A., Southon, J.R., Talamo, S., Turney, #.C.S.M., J.v.d.P., Weyhenmeyer, C.E., 2009. INTCAL09 and MARINE09 radiocarbon age calibration curves, 0–50,000 years Cal BP. Radiocarbon 51, 1111–1150.
Rein, B., Sirocko, F., 2002. In-situ reflectance spectroscopy — analysing techniques for high-resolution pigment logging in sediment cores. International Journal of Earth Sciences 91, 950–954.
Renema, W., 2006. Large benthic foraminifera from the deep photic zone of a mixed siliciclastic-carbonate shelf off East Kalimantan, Indonesia. Marine Micropaleontology 58, 73.
Ryan, D.A., Bostock, H.C., Brooke, B.P., Marshall, J.F., 2007. Bathymetric expression of the Fitzroy River palaeochannel, northeast Australia: response of a major river to sea-level change on a semi-rimmed, mixed siliciclastic-carbonate shelf. Sedimentary Geology 201, 196–211.
Schlager, W., Reijmer, J.J.G., Droxler, A., 1994. Highstand shedding of carbonate platforms. Journal of Sedimentary Research 64, 270–281.
Schröder-Adams, C.J., Boyd, R., Ruming, K., Sandstrom, M., 2008. Influence of sediment transport dynamics and ocean floor morphology on benthic foraminifera, offshore Fraser Island, Australia. Marine Geology 254, 47–61.
Shanmugam, G., 2002. Ten turbidite myths. Earth-Science Reviews 58, 311–341.
Siddall, M., Rohling, E.J., Thompson, P.R., Waelbroeck, C., 2008. Marine isotope stage 3 sea level fluctuations: data synthesis and new outlook. Review of Geophysics 46. doi:10.1029/2007RG000226.
Thompson, W.G., Goldstein, S.L., 2006. A radiometric calibration of the SPECMAP timescale. Quaternary Science Reviews 25, 3207–3215.
Watts, K.F., Varga, L.L., Feary, D.A., 1993. Origins, timing and implications of Miocene to Pleistocene turbidites, debris flows, and slump deposits of the Queensland Trough, Northeastern Australia (Site 823). In: McKenzie, J.A., Davies, P.J., Palmer-Julson, A. (Eds.), Proc. ODP. Sci. Results. Ocean Drilling Program, College Station, TX, pp. 379–406.
Webster, J.M., Davies, P.J., Beaman, R.J., Williams, S., Byrne, M., 2008. Evolution of drowned shelf edge reefs in the GBR; implications for understanding abrupt climate change, coral reef response and modern deep water benthic habitats. RV Southern Survey — Voyage Summary: Marine National Facility, 18. http://www.marine.csiro.au/nationalfacility/voyagedocs/2007/summarySS2007-2007.pdf.
Weninger, B., Joris, O., Danzeglocke, U., 2007. CalPal-2007. Cologne Radiocarbon Calibration & Palaeoclimate Research Package.
Williams, M., Cook, E., van der Kaars, S., Barrows, T., Shulmeister, J., Kershaw, P., 2009. Glacial and deglacial climatic patterns in Australia and surrounding regions from 35,000 to 10,000 years ago reconstructed from terrestrial and near-shore proxy data. Quaternary Science Reviews 28, 2398–2419.
Wilson, J.L., 1967. Cyclic and reciprocal sedimentation in Virgilian Strata of Southern New Mexico. Geological Society of America Bulletin 78, 805–818.
Woolfe, K., Larcombe, P., Naish, T.R., Purdon, R., 1998. Lowstand rivers need not incise the shelf: an example from the Great Barrier Reef, Australia, with implications for sequence stratigraphic models. Geology 26, 75–78.
Wynn, R.B., Stow, D.A.V., 2002. Classification and characterisation of deep-water sediment waves. Marine Geology 192, 7–22.
Xu, J.P., Wong, F.L., Kvitek, R., Smith, D.P., Paull, C.K., 2008. Sandwave migration in Monterey Submarine Canyon, Central California. Marine Geology 248, 193–212.
Yokoyama, Y., Webster, J.M., Cotterill, C., Braga, J.C., Jovane, L., Mills, H., Morgan, S., Suzuki, A., Scientists, a.E., 2011. IODP Expedition 325: Great Barrier Reefs reveals past sea-level, climate and environmental changes during the end of the last Ice age. Scientific Drilling 12, 32–45.